Zegao Wang, Pingjian Li, Yuanfu Chen, Jiarui He, Wanli Zhang, Oliver G. Schmidt, Yanrong Li

Pure thiophene–sulfur doped reduced graphene oxide: synthesis, structure, and electrical properties

Erstveröffentlichung in / First published in:
Nanoscale. 2014, 6(13), S. 7281–7287 [Zugriff am: 04.11.2019]. Royal Society of Chemistry. ISSN 2040-3372.

DOI: https://doi.org/10.1039/c3nr05061k

Nanoscale

PAPER

View Article Online
View Journal | View Issue

Cite this: *Nanoscale*, 2014, **6**, 7281

Pure thiophene–sulfur doped reduced graphene oxide: synthesis, structure, and electrical properties†

Zegao Wang,[a] Pingjian Li,*[a] Yuanfu Chen,*[a] Jiarui He,[a] Wanli Zhang,[a] Oliver G. Schmidt[bc] and Yanrong Li[a]

Received 23rd September 2013
Accepted 8th January 2014

DOI: 10.1039/c3nr05061k

www.rsc.org/nanoscale

Here we propose, for the first time, a new and green ethanol-thermal reaction method to synthesize high-quality and pure thiophene–sulfur doped reduced graphene oxide (rGO), which establishes an excellent platform for studying sulfur (S) doping effects on the physical/chemical properties of this material. We have quantitatively demonstrated that the conductivity enhancement of thiophene–S doped rGO is not only caused by the more effective reduction induced by S doping, but also by the doped S atoms, themselves. Furthermore, we demonstrate that the S doping is more effective in enhancing conductivity of rGO than nitrogen (N) doping due to its stronger electron donor ability. Finally, the dye-sensitized solar cell (DSCC) employing the S-doped rGO/TiO_2 photoanode exhibits much better performance than undoped rGO/TiO_2, N-doped rGO/TiO_2 and TiO_2 photoanodes. It therefore seems promising for thiophene–S doped rGO to be widely used in electronic and optoelectronic devices.

Introduction

Graphene, a new two-dimensional nanomaterial, has attracted huge attention due to its outstanding properties and broad range of potential applications.[1–5] Among the various synthesis methods of graphene, chemical reduction of graphene oxide (GO) is a particular promising way to produce graphene in large volumes. However, the low conductivity of reduced GO (rGO) renders practical applications into the realm of eventuality, such as graphene/TiO_2 electrodes in dye-sensitized solar cells (DSSCs),[6–8] graphene-based electrodes in Li-ion batteries or super capacitors,[9–11] or transparent conductive electrodes in optoelectronic devices.[12–15]

There are already many efforts to control the electrical performance of rGO,[16–19] and heteroatom doping is considered as one of the most effective ways to modulate the band structure and improve the electrical properties of graphene.[20–24] So far, it has been reported that nitrogen (N) or boron (B) doping can effectively increase the electrical conductivity of rGO, and the reason was mainly due to the more effective GO reduction caused by heteroatom doping.[22–24] However, it is still unclear whether doped N (or B) atoms can contribute to the conductivity enhancement of rGO, because doped atoms cause the decrease in mobility while increasing the carrier concentration of rGO.

Besides N and B doping, theoretical calculations suggest that sulfur (S) doping can also modulate the electron structure of graphene.[25] However, because the S atoms incorporated into graphene requires a larger formation energy than N or B atoms,[25] the synthesis of S-doped rGO is more difficult. Although recently the synthesis of S-doped rGO by thermal annealing reduction has been reported,[26–28] the electrical properties of S-doped rGO remain entirely unexplored. In addition, all the reported S-doped rGO samples have two types of S-bonding configurations (thiophene–S and oxidized S).[26–28] This hinders a conclusive study of the doping effect of S on the physical and chemical properties of rGO, because the different types of S-bonding configurations correspond to different properties.

Here we propose a new and environmentally friendly method to synthesize S-doped rGO with pure thiophene–S bonding configuration. The S doping and chemical reduction are achieved simultaneously by the ethanol-thermal reaction. The studies reveal that S doping can effectively facilitate the GO reduction and increase the electrical conductivity of rGO. Furthermore, we demonstrate that the conductivity enhancement is not only caused by the more effective reduction of GO, but also directly by the S dopants, themselves. In addition, we also demonstrate that S doping is more effective in enhancing the conductivity of rGO than N doping. To the best of our knowledge, it is the first time that the ethanol-thermal S doping and reduction mechanisms of GO are reported, and the effect of

[a]*State Key Laboratory of Electronic Thin Films and Integrated Devices, University of Electronic Science and Technology of China, Chengdu 610054, P. R. China. E-mail: yfchen@uestc.edu.cn; lipingjian@uestc.edu.cn; Fax: +86-028-83202710; Tel: +86-028-83202710*

[b]*Institute for Integrative Nanosciences, IFW Dresden, Helmholtzstrasse 20, 01069 Dresden, Germany*

[c]*Center for Advancing Electronics Dresden, TU Dresden, 01062 Dresden, Germany*

† Electronic supplementary information (ESI) available. See DOI: 10.1039/c3nr05061k

S doping on the electrical properties of rGO is investigated. Moreover, as a potential application, we have investigated the DSSC employing the S-doped rGO/TiO_2 photoanode, which shows better performance than undoped rGO/TiO_2, N-doped rGO/TiO_2 and TiO_2 photoanodes.

Results and discussions

In this study, the S-doped rGO was synthesized by S doping and GO reduction *via* the ethanol-thermal reaction. Benzyl disulfide and ethanol were used as S doping source and reducing agent, respectively; the ethanol-thermal temperature was 180 °C. For comparison, undoped rGO was synthesized by the same procedure except that the S doping source (benzyl disulfide) was absent. The as-synthesized S-doped rGO and undoped rGO samples are denoted as S-rGO-*X* and rGO-*X*, respectively, where *X* represents the ethanol-thermal reaction time (h). The S-rGO-10 h was firstly characterized by transmission electron microscopy (TEM) with energy dispersive X-ray spectrometry (EDX) and scanning transmission electron microscopy (STEM).

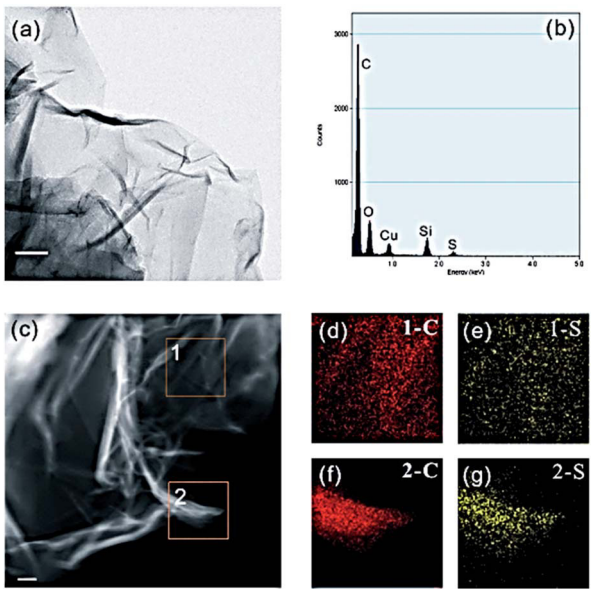

Fig. 1 (a–c) TEM image, EDX spectrum and STEM image of S-rGO-10 h, respectively. (d) C- and (e) S-elemental mapping of square region 1 in (c). (f) C- and (g) S-elemental mapping of square region 2 in (c). The scale bars in (a) and (c) are 100 and 50 nm, respectively.

Fig. 1a shows a typical TEM image of S-rGO-10 h. The image reveals transparent graphene sheets with wrinkle and fold features, which may originate from defective structures formed during the S doping and reduction process of GO. The corresponding EDX spectrum (Fig. 1b) confirms the presence of S atoms in S-rGO-10 h (the Si peak in Fig. 1b originates from the Si (Li) detectors). Fig. 1c–g represent the STEM elemental mappings of S-rGO-10 h, which show that the doped S atoms are homogeneously distributed in the plane of graphene; the similar C and S mappings reveal that the doped S atoms are incorporated into not only the plane but also the edge of graphene.

In order to investigate the elemental composition and S-bonding configurations in S-rGO-10 h, the X-ray photoelectron spectroscopy (XPS) measurements were performed at room temperature. As shown in Fig. 2a, the S peak appears and the intensity of O peak decreases in the XPS spectrum of S-rGO-10 h compared to GO. It indicates that the S atoms are incorporated into rGO and the large amounts of oxygen-functional groups (C–O bonds, carbonyls, or carboxylates) on GO are removed during the ethanol-thermal reaction. It is noted that the possibility of physical adsorption of S onto the samples is excluded by the following two reasons: (1) the samples were ultrasonically dispersed in various solvents like ethanol, acetone, and H_2O; the XPS results reveal no change in the S level before and after sonication (XPS data not shown). (2) When the ethanol-thermal reaction time is smaller than 1 h, any S-related XPS signal is below the detection limit, as shown in the inset of Fig. 2b.

Fig. 2b is the high resolution S2p XPS spectrum of S-rGO-10 h. The S2p peak can be deconvoluted into two peaks at binding energies of ~164.0 eV and ~165.3 eV, which correspond to the $S2p_{3/2}$ and $S2p_{1/2}$ energy positions of thiophene–S, respectively.[27,29] More importantly, we do not detect other S components such as thiol (SH) at around 162.0 eV,[29] or oxidized S at around 167–169 eV.[26–28,30,31] It is the first time to synthesize

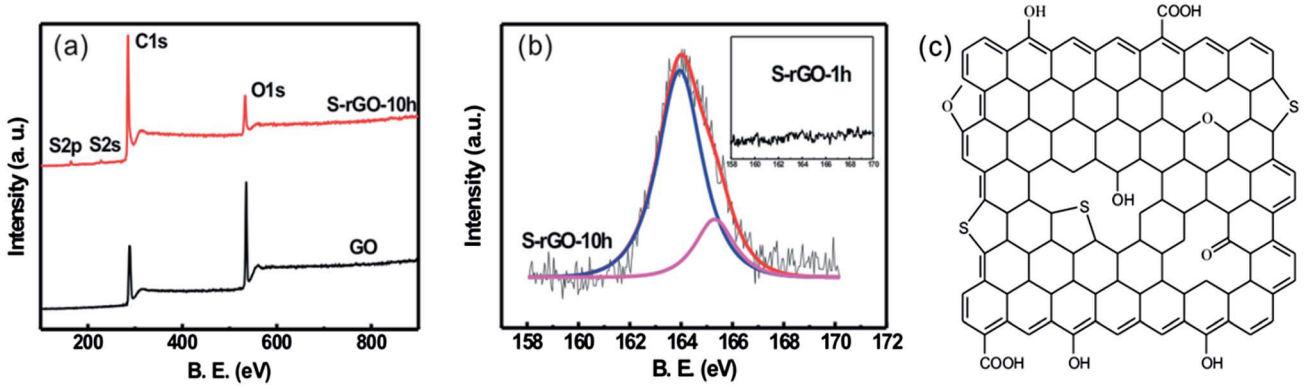

Fig. 2 (a) XPS spectra of GO and S-rGO-10 h. (b) High resolution S2p XPS spectrum of S-rGO-10 h, and the inset shows the S2p XPS spectrum of S-rGO-1 h. (c) Schematic structure of pure thiophene–S doped rGO.

the S-doped rGO with only one kind of S-bonding configurations, which can serve as an excellent platform to study doping effects of the physical and chemical properties of S-doped rGO. In addition, the S content (thiophene–S) of S-rGO-10 h is 1.2 at%, which is comparable to that of S-doped rGO synthesized by thermal annealing reduction (see ESI Table S1†).[26–28]

In order to investigate the ethanol-thermal S doping and GO reduction mechanisms, we have studied the influence of the ethanol-thermal reaction time t_{etr} on the elemental composition of S-doped rGO by XPS analysis. Fig. 3a and b show the S and O contents in S-doped rGO as a function of t_{etr} at 180 °C, respectively. When $t_{etr} \leq 1$ h, any S-related XPS signal is below the detection limit, which implies that the S doping requires sufficient reaction time. For $t_{etr} = 2$–10 h, we observe an increase in the S content and, at the same time, a decrease in the O content, suggesting that S doping and GO reduction are achieved simultaneously during the ethanol-thermal reaction. When $t_{etr} = 10$ h, the S content reaches a maximum value of 1.2 at%. For $t_{etr} > 10$ h, the O content remains nearly unchanged, *i.e.* the GO reduction ceases. However, and more significantly, the S content starts to decrease with increasing reaction time, which indicates that excessive ethanol-thermal treatment can cause the breakage of C–S bonds and the removal of S atoms. A similar phenomenon was also observed in previous reports for the breakage of C–N bonds in N-doped graphene caused by overheating.[21,32]

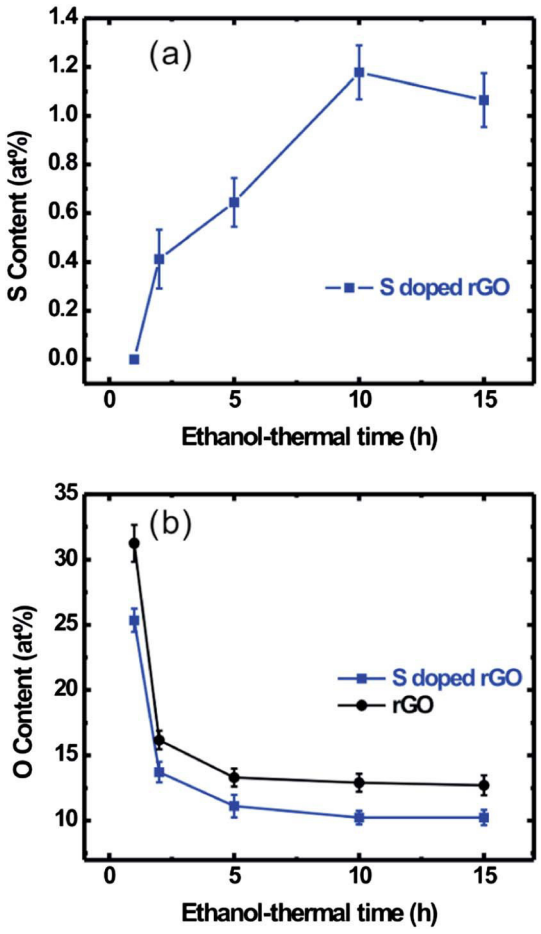

Fig. 3 The investigations of elemental compositions of S-doped rGO and undoped rGO synthesized *via* ethanol-thermal reaction by XPS analysis. (a) S and (b) O contents as a function of ethanol-thermal time at 180 °C. The values are mean and standard deviation (error bars) for 5 different samples.

For further investigating the effect of S doping on the degree of GO reduction, we have studied the O content of undoped rGO synthesized by ethanol-thermal reaction for comparison. As shown in Fig. 3b, the O content of S-doped rGO is obviously smaller than that of undoped rGO synthesized at the same ethanol-thermal time. It therefore seems that the S doping occurs preferably at the sites of oxygen-functional groups in GO, thus affording a more effective reduction of GO. This phenomenon is similar to the case of N doping and reduction of GO.[21,32] More interestingly, it is noted that when $t_{etr} = 1$ h, however the S level is below the detection limit, the presence of S source still causes the more effective GO reduction. It implies that the S source can be acted as the catalyst for GO reduction at the beginning of the ethanol-thermal reaction.

In addition, it is known that besides the doping content, the doping structures have also influenced the properties of rGO, thus we have further studied the effect of the ethanol-thermal reaction time on the bonding configuration of S atoms. As shown in Fig. S1 in ESI,† all high resolution S2p XPS spectra of S-doped rGO samples synthesized at various ethanol-thermal time show the pure thiophene–S bonding configuration. This implies that the ethanol-thermal reaction effectively prevents the formation of oxidized S, which was formed in the S-doped rGO samples synthesized by thermal annealing reduction.[26–28] The reason may be that the large amounts of oxygen-functional groups have already been removed before the S atoms are incorporated into rGO (discussed in the previous paragraph), and the definite conclusion needs to be further investigated. Moreover, because the oxidized S may cause a decrease in the conductivity of carbon materials,[33] we expect the ethanol-thermal reaction method to be a more effective way to synthesize S-doped rGO with high conductivity.

In order to investigate the effect of S doping on the electrical properties of rGO, Hall measurements were conducted at room temperature (the experimental details are given in Experimental section). Among all S-doped rGO samples, the S-rGO-10 h has the highest value of conductivity (see ESI Fig. S2†). As shown in Fig. 4a and Table 1, the S doping causes the ~321% increase in conductivity from rGO-10 h to S-rGO-10 h, given by eqn (1), where $\sigma_{\text{S-rGO-10 h}}$ and $\sigma_{\text{rGO-10 h}}$ are the conductivity of S-rGO-10 h and rGO-10 h, respectively.

$$\frac{\sigma_{\text{S-rGO-10 h}} - \sigma_{\text{rGO-10 h}}}{\sigma_{\text{rGO-10 h}}} \quad (1)$$

However, because the S doping not only introduces S atoms into rGO but also causes a more effective reduction of GO (Fig. 3 and Table 1), it is hard to distinguish the effect of S and O on the conductivity of S-doped rGO. In view of this, for comparison, we have introduced the new undoped rGO sample, which was synthesized by the two-step chemical reduction process (denoted as rGO-TS),[16] and the experimental details are given in the

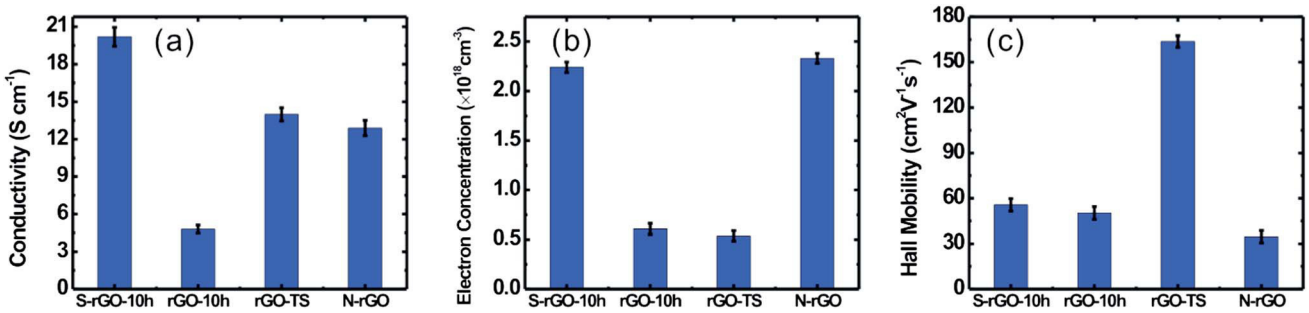

Fig. 4 (a) Conductivities, (b) electron concentrations and (c) Hall mobilities of S-rGO-10 h, rGO-10 h, rGO-TS, and N-rGO. The values are mean and standard deviation (error bars) for 5 different samples.

Table 1 Elemental composition and conductivity of S-rGO-10 h, rGO-10 h, rGO-TS, and N-rGO. The values are mean and standard deviation (error bars) for 5 different samples

	O (at%)		S (at%)		N (at%)		Conductivity (S cm^{-1})	
	Mean	SD	Mean	SD	Mean	SD	Mean	SD
S-rGO-10 h	10.2	0.49	1.2	0.11	—	—	20.2	0.76
rGO-10 h	12.9	0.61	—	—	—	—	4.8	0.32
rGO-TS	10.4	0.41	—	—	—	—	14.0	0.53
N-rGO	10.2	0.56	—	—	4.2	0.29	12.9	0.61

Experimental section. By introducing rGO-TS, eqn (1) can be equal to the sum of eqn (2) and (3), where $\sigma_{\text{rGO-TS}}$ is the conductivity of rGO-TS.

$$\frac{\sigma_{\text{S-rGO-10 h}} - \sigma_{\text{rGO-TS}}}{\sigma_{\text{rGO-10 h}}} \quad (2)$$

$$\frac{\sigma_{\text{rGO-TS}} - \sigma_{\text{rGO-10 h}}}{\sigma_{\text{rGO-10 h}}} \quad (3)$$

Because the S-rGO-10 h and rGO-TS have similar O content (Table 1) and O-bonding configurations (Fig. S3 and Table S2 in ESI†), eqn (2) and (3) can be used for estimating the contributions of doped S atoms and the more effective GO reduction (induced by S doping) on the increase in conductivity from rGO-10 h to S-rGO-10 h, respectively. As a result, the doped S atoms contribute to the ~129% increase in conductivity (eqn (2)). It is attributed that the increase in electron concentration caused by S doping (n-type doping), is larger than the decrease in mobility originating from S-related defects (thiophene–S), as shown in Fig. 4b and c. On the other hand, the more effective GO reduction caused by S doping contributes to the ~192% increase in conductivity (eqn (3)). It is mainly due to the removing of more oxygen-functional groups, which is consistent with previous reports.[16,18,34]

In order to further evaluate the enhancement effect of S doping on the conductivity of rGO, the electrical properties of 4.2 at% N-doped rGO (see ESI Fig. S4†) have been studied, which was synthesized by the hydrazine reduction (denoted as N-rGO),[35] and the experimental details are given in the Experimental section. From Fig. 4a, we find that the S-rGO-10 h has an obvious higher conductivity than N-rGO, which can be explained as follows: (1) the S-rGO-10 h and N-rGO samples have similar O content (Table 1), which implies that the S and N doping afford the comparable promoting effects on the GO reduction. Thus, the conductivity difference between S-rGO-10 h and N-rGO is mainly originated from the different effects of doped S and N atoms. (2) As shown in Fig. 4b, compared to rGO-TS, the 1.2 at% S (S-rGO-10 h) and 4.2 at% N atoms (N-rGO) cause comparable increases in electron concentration, indicating that the electron donor ability of S atoms is stronger than that of N atoms. (3) As shown in Fig. 4c, compared to rGO-TS, the S atoms cause a smaller decrease in mobility than N atoms, which is due to the fewer defects caused by lower S content. As a result, compared to rGO-TS, the doped S atoms causes an obvious increase while the doped N atoms cause a slightly decrease in the rGO conductivity, as shown in Fig. 4a. Thus, we conclude that the S doping is more effective to increase the conductivity of rGO than N doping. Our studies also reveal that the doped atoms do not necessarily increase the conductivity of rGO, thus introducing the doped atoms or structures, with stronger electron donor ability or lower carrier scattering, will be the key to increase the rGO conductivity.

Because of the conductivity enhanced by S doping, the thiophene–S doped rGO will be widely used in electronic and optoelectronic devices. As one kind of potential application, we have investigated the photoelectrical properties of DSSCs employing S-doped rGO/TiO_2 photoanodes. Fig. 5a shows the electrochemical impedance spectra (EIS) of DSSCs employing S-rGO-10 h/TiO_2, rGO-TS/TiO_2, N-rGO/TiO_2, rGO-10 h/TiO_2 and TiO_2 photoanodes, and corresponding charge transfer resistances (R_{ct}) are 5.70, 11.01, 13.47, 16.84, and 17.58 Ω cm^2, respectively, as shown in Table 2. As anticipated, the variation of

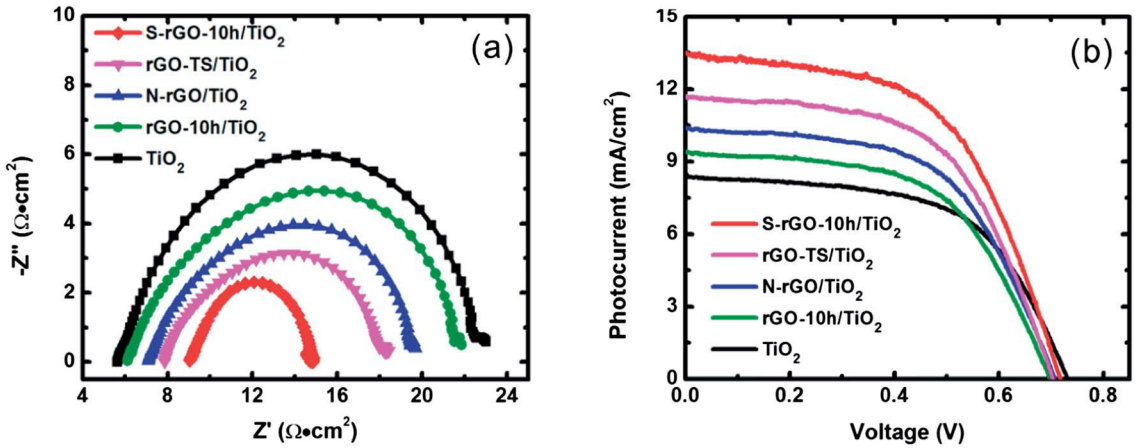

Fig. 5 (a) EIS of S-rGO-10 h/TiO_2, rGO-TS/TiO_2, N-rGO/TiO_2, rGO-10 h/TiO_2 and TiO_2 photoanodes. (b) Photocurrent density–voltage characteristics of DSSCs employing S-rGO-10 h/TiO_2, rGO-TS/TiO_2, N-rGO/TiO_2, rGO-10 h/TiO_2 and TiO_2 photoanodes.

Table 2 Photovoltaic performance parameters of DSSCs employing S-rGO-10 h/TiO_2, rGO-TS/TiO_2, N-rGO/TiO_2, rGO-10 h/TiO_2 and TiO_2 photoanodes. The values are mean and standard deviation (SD) for 5 different samples

	I_{SC} (mA cm^{-2})		V_{OC} (V)		η		R_{ct} (Ω cm^2)	
	Mean	SD	Mean	SD	Mean	SD	Mean	SD
S-rGO-10 h/TiO_2	13.51	0.067	0.72	0.009	5.32%	0.054%	5.70	0.102
rGO-TS/TiO_2	11.71	0.052	0.70	0.007	4.65%	0.098%	11.01	0.219
N-rGO/TiO_2	10.42	0.050	0.71	0.012	4.17%	0.056%	13.47	0.182
rGO-10 h/TiO_2	9.42	0.035	0.70	0.009	3.72%	0.061%	16.84	0.329
TiO_2	8.50	0.042	0.73	0.011	3.57%	0.045%	17.58	0.519

R_{ct} is consistent with the resistance of graphene shown in Table 1, and the S-rGO-10 h/TiO_2 photoanode with highest conductivity has the lowest R_{ct}. It demonstrates that introducing graphene effectively improves the conductive path through the TiO_2 matrix, and the S-rGO-10 h causes the greatest improvement due to its highest conductivity. As a result, when S-rGO-10 h was introduced into the TiO_2 photoanode, the DSSC has the highest short-circuit photocurrent density (I_{sc}) and conversion efficiency (η), which are 13.51 mA cm^{-2} and 5.32%, respectively, as shown in Fig. 5b and Table 2. Compared to the TiO_2 photoanode, the DSSC employing the S-rGO-10 h/TiO_2 photoanode has a ~49% increase in conversion efficiency, which reveals the significant improvement of performance of DSSCs by introducing S-doped rGO.

Experimental

Synthesis of S-doped rGO by ethanol-thermal reduction

GO was synthesized from flake graphite (Qingdao Tianhe Graphite Co. Ltd, Qingdao, China) by a modified Hummers method.[36,37] To prepare S-doped rGO, 0.125 g benzyl disulfide was dissolved into 50 mL ethanol, and then 1 g GO was added. After the solution was stirred and dispersed in ultrasonic cleaner for about 1 h, it was transferred into a Teflon-lined autoclave and heated at 180 °C for 1–15 h. Finally, the S-doped rGO was obtained by filtering and washing with warm ethanol several times.

Synthesis of undoped rGO by ethanol-thermal reduction

The undoped rGO was synthesized with similar procedure of S-doped rGO, just not adding the benzyl disulfide.

Synthesis of undoped rGO by two-step reduction

The GO was reduced using $NaBH_4$ and concentrated H_2SO_4 which is similar with ref. 16. Firstly, GO was dispersed in DI water to give a 1 mg mL^{-1} colloidal solution. The pH of this solution was then adjusted to 9–10 by sodium carbonate solution. 0.8 g sodium borohydride was directly added into 1 L GO dispersion under magnetic stirring, and the mixture was held at 80 °C for 1 h. Filtered and washed with large amounts of water several times, and then dried in vacuum for two days. This partially rGO was redispersed in concentrated sulfuric acid and heated to 120 °C for 12 h. After cooling, the dispersion was diluted with DI water, filtered and rinsed with water to remove impurities. The final product was denoted as rGO-TS.

Synthesis of N-doped rGO by hydrazine reduction

The GO was reduced using hydrazine monohydrate which is similar with ref. 35. 1 L GO solution (1 mg mL^{-1}) was prepared and then 1 mL hydrazine monohydrate (80%) was subsequently added into the suspension. Additional stirring with a stirring bar in a water-bath held at 80 °C for 10 h. After cooling to room temperature, the solution was filtered and washed by water, and finally dried in vacuum. The final product was denoted as N-rGO.

Preparation of DSSCs with different photoanodes

The TiO_2 was purchased from Dalian Heptachroma SolarTech Co., Ltd. To prepare the S-rGO-10 h/TiO_2 photoanode, 2 mg SrGO-10 h and 1 g TiO_2 were added into 20 mL DI water with

1 mL acetylacetone and 1.5 mL emulsifier-OP. After the solution was stirred at 60 °C for 3 h, the resulting paste was coating on fluorine-doped tin oxide (FTO) conductive glass using doctor-blading technique. Finally, the S-rGO-10 h/TiO_2 photoanode was obtained by annealing in air at 500 °C for 30 min. For comparison, the rGO-TS/TiO_2, N-rGO/TiO_2, rGO-10 h/TiO_2 and TiO_2 photoanodes were fabricated with similar procedure of S-rGO-10 h/TiO_2 photoanode. For DSSCs fabrication, the above five types of photoanodes were sensitized by immersing into an ethanol solution containing the 0.5 mM N719 dye solution (Dalian Heptachroma SolarTech Co., Ltd.) for 10 h. The counter electrode was the 100 nm Pt film which was sputtering on FTO. The DSSC was made of a photoanode, a counter electrode and an electrolyte solution (DHS-E23, Dalian Heptachroma SolarTech Co. Ltd). The electrode area was 0.25 cm^2.

Characterization

The TEM and STEM images were taken with an FEI Tecnai G2 microscope. XPS was performed on a Kratos XSAM800 using Al Ka radiation (144 W, 12 mA, 12 kV). For studying the electrical properties of powder samples, they were compressed into films at 20 MPa with thickness of ~700 um and bulk densities of ~1.4 g cm^{-3}, and the Hall measurements (HMS-2000, Ecopia) were performed under ambient condition at room temperature. The EIS spectra were captured in the frequency range of 0.1 Hz to 1 MHz with 0.01 V applied AC voltage in a two-electrode system on an electrochemical workstation (CHI660D, Chenhua Instruments Co., Shanghai). The photocurrent density–voltage characteristics of DSSCs were measured using a Keithley-2000 and Yokogawa-7651 source meters under the excitation of 100 mW cm^{-2} AM 1.5 white light from a solar simulator (XQ350W, Shanghai lansheng electronic Co., Ltd.).

Conclusions

In conclusion, we synthesized the pure thiophene–S doped rGO by a simple and environmentally friendly ethanol-thermal reaction, in which benzyl disulfide and ethanol were used as S doping source and reducing agent, respectively. The TEM and XPS studies confirm the S doping, and also reveal that S atoms are incorporated into rGO with only one kind of S-bonding configuration (thiophene–S). Further, the studies show that the S doping and GO reduction are simultaneously achieved, and the S doping can effectively promote the GO reduction. More significantly, the Hall effect studies indicate that S doping can effectively increase the conductivity of rGO, which is caused not only by the more effective GO reduction, but also directly by the doped S atoms, themselves. Further, we have demonstrated that S doping is more effective in increasing the rGO conductivity than N doping, which is due to the stronger electron donor ability of S atoms. As a potential application, we have investigated the photoelectrical properties of DSSC employing S-doped rGO/TiO_2 photoanode. Owing to the conductivity enhancement effect induced by S doping, the DSSC employing S-doped rGO/TiO_2 photoanode shows a higher performance than that employing undoped rGO/TiO_2, N-doped rGO/TiO_2, and TiO_2 photoanodes. We are convinced that the thiophene–S doped rGO not only will be widely used in electronic and optoelectronic devices, but also establish an excellent platform for studying S doping effects on the physical/chemical properties of rGO due to its single type of C–S bonds.

Acknowledgements

Z. G. W., P. J. L., and Y. F. C. contributed equally to this work. The research was supported by the National Natural Science Foundation of China (Grant no. 51372033 and no. 51202022), the Program for New Century Excellent Talents in University (Grant no. NCET-10-0291), the 111 Project (Grant no. B13042), the Specialized Research Fund for the Doctoral Program of Higher Education of China (Grant no. 20120185120011), the Fundamental Research Funds for the Central Universities (Grant no. ZYGX2010J031), and the Startup Research Project of University of Electronic Science and Technology of China (Grant no. Y02002010301041). We thank associate Prof. Ming Liu of Analysis and Testing Center, Sichuan University for her technical help for TEM characterization.

Notes and references

1 A. K. Geim, *Science*, 2009, **324**, 1530–1534.
2 I. K. Moon, J. Lee, R. S. Ruoff and H. Lee, *Nat. Commun.*, 2010, **1**, 73.
3 Z. G. Wang, Y. F. Chen, P. J. Li, X. Hao, J. B. Liu, R. Huang and Y. R. Li, *ACS Nano*, 2011, **5**, 7149–7154.
4 Y. M. Lin, A. Valdes-Garcia, S. J. Han, D. B. Farmer, I. Meric, Y. N. Sun, Y. Q. Wu, C. Dimitrakopoulos, A. Grill, P. Avouris and K. A. Jenkins, *Science*, 2011, **332**, 1294–1297.
5 Y. W. Zhu, S. Murali, M. D. Stoller, K. J. Ganesh, W. W. Cai, P. J. Ferreira, A. Pirkle, R. M. Wallace, K. A. Cychosz, M. Thommes, D. Su, E. A. Stach and R. S. Ruoff, *Science*, 2011, **332**, 1537–1541.
6 N. Li, G. Liu, C. Zhen, F. Li, L. L. Zhang and H. M. Cheng, *Adv. Funct. Mater.*, 2011, **21**, 1717–1722.
7 N. L. Yang, J. Zhai, D. Wang, Y. S. Chen and L. Jiang, *ACS Nano*, 2010, **4**, 887–894.
8 L. Kavan, J. H. Yum and M. Gratzel, *Nano Lett.*, 2011, **11**, 5501–5506.
9 X. F. Zhou, F. Wang, Y. M. Zhu and Z. P. Liu, *J. Mater. Chem.*, 2011, **21**, 3353–3358.
10 X. Zhao, C. M. Hayner, M. C. Kung and H. H. Kung, *Adv. Energy Mater.*, 2011, **1**, 1079–1084.
11 M. J. Zhi, C. C. Xiang, J. T. Li, M. Li and N. Q. Wu, *Nanoscale*, 2013, **5**, 72–88.
12 D. H. Lee, H. J. Lee, Y. M. Ahn, Y. J. Jeong, D. Y. Lee and Y. G. Lee, *Nanoscale*, 2013, **5**, 7750–7755.
13 Z. Y. Yin, S. Y. Sun, T. Salim, S. X. Wu, X. Huang, Q. Y. He, Y. M. Lam and H. Zhang, *ACS Nano*, 2010, **4**, 5263–5268.
14 X. Wang, L. J. Zhi and K. Mullen, *Nano Lett.*, 2008, **8**, 323–327.
15 G. Eda, G. Fanchini and M. Chhowalla, *Nat. Nanotechnol.*, 2008, **3**, 270–274.

16 W. Gao, L. B. Alemany, L. J. Ci and P. M. Ajayan, *Nat. Chem.*, 2009, **1**, 403–408.
17 J. P. Zhao, S. F. Pei, W. C. Ren, L. B. Gao and H. M. Cheng, *ACS Nano*, 2010, **4**, 5245–5252.
18 M. H. Jin, T. H. Kim, S. C. Lim, D. L. Duong, H. J. Shin, Y. W. Jo, H. K. Jeong, J. Chang, S. S. Xie and Y. H. Lee, *Adv. Funct. Mater.*, 2011, **21**, 3496–3501.
19 I. N. Kholmanov, M. D. Stoller, J. Edgeworth, W. H. Lee, H. F. Li, J. Lee, C. Barnhart, J. R. Potts, R. Piner, D. Akinwande, J. E. Barrick and R. S. Ruoff, *ACS Nano*, 2012, **6**, 5157–5163.
20 T. B. Martins, R. H. Miwa, A. J. R. Da Silva and A. Fazzio, *Phys. Rev. Lett.*, 2007, **98**, 196803–196806.
21 X. L. Li, H. L. Wang, J. T. Robinson, H. Sanchez, G. Diankov and H. J. Dai, *J. Am. Chem. Soc.*, 2009, **131**, 15939–15944.
22 Z. S. Wu, W. C. Ren, L. Xu, F. Li and H. M. Cheng, *ACS Nano*, 2011, **5**, 5463–5471.
23 T. V. Khai, H. G. Na, D. S. Kwak, Y. J. Kwon, H. Ham, K. B. Shim and H. W. Kim, *J. Mater. Chem.*, 2012, **22**, 17992–18003.
24 M. Y. Yen, C. K. Hsieh, C. C. Teng, M. C. Hsiao, P. I. Liu, C. C. M. Ma, M. C. Tsai, C. H. Tsai, Y. R. Lin and T. Y. Chou, *RSC Adv.*, 2012, **2**, 2725–2728.
25 P. A. Denis, R. Faccio and A. W. Mombru, *ChemPhysChem*, 2008, **10**, 715–722.
26 Z. Yang, Z. Yao, G. F. Li, G. Y. Fang, H. G. Nie, Z. Liu, X. M. Zhou, X. A. Chen and S. M. Huang, *ACS Nano*, 2012, **6**, 205–211.
27 S. B. Yang, L. J. Zhi, K. Tang, X. L. Feng, J. Maier and K. Mullen, *Adv. Funct. Mater.*, 2012, **22**, 3634–3640.
28 H. L. Poh, P. Simek, Z. Sofer and M. Pumera, *ACS Nano*, 2013, **7**, 5262–5272.
29 F. Buckel, F. Effenberger, C. Yan, A. Golzhauser and M. Grunze, *Adv. Mater.*, 2000, **12**, 901–905.
30 I. Herrmann, U. I. Kramm, J. Radnik, S. Fiechter and P. Bogdanoff, *J. Electrochem. Soc.*, 2009, **156**, B1283–B1292.
31 J. Y. Kim, P. J. Reucroft, M. Taghiei, V. R. Pradhan and I. Wender, *Energy Fuels*, 1994, **8**, 886–889.
32 T. N. Huan, T. V. Khai, Y. J. Kang, K. B. Shim and H. Chung, *J. Mater. Chem.*, 2012, **22**, 14756–14762.
33 J. Y. Ji, G. H. Zhang, H. Y. Chen, S. L. Wang, G. L. Zhang, F. B. Zhang and X. B. Fan, *Chem. Sci.*, 2011, **2**, 484–487.
34 S. F. Pei and H. M. Cheng, *Carbon*, 2012, **50**, 3210–3228.
35 S. Park, J. H. An, J. R. Potts, A. Velamakanni, S. Murali and R. S. Ruoff, *Carbon*, 2011, **49**, 3019–3023.
36 N. I. Kovtyukhova, P. J. Ollivier, B. R. Martin, T. E. Mallouk, S. A. Chizhik, E. V. Buzaneva and A. D. Gorchinskiy, *Chem. Mater.*, 1999, **11**, 771–778.
37 W. S. Hummers and R. E. Offeman, *J. Am. Chem. Soc.*, 1958, **80**, 1339.